ORNL/TM-2020/1548

Technical Qualification of New Materials for High Efficiency Coal-Fired Boilers and Other Advanced FE Concepts: Haynes® 282® ASME Boiler and Pressure Vessel Code Case

Bruce A. Pint
Hong Wang
C. Shane Hawkins
Kinga A. Unocic

June 2020

OAK RIDGE NATIONAL LABORATORY
MANAGED BY UT-BATTELLE FOR THE US DEPARTMENT OF ENERGY

ORNL/TM-2020/1548

Materials Science and Technology Division

TECHNICAL QUALIFICATION OF NEW MATERIALS FOR HIGH EFFICIENCY COAL-FIRED BOILERS AND OTHER ADVANCED FE CONCEPTS: HAYNES® 282® ASME BOILER AND PRESSURE VESSEL CODE CASE

Bruce A. Pint, Hong Wang, C. Shane Hawkins, and Kinga A. Unocic

Date Published: June 2020

Prepared by
OAK RIDGE NATIONAL LABORATORY
Oak Ridge, TN 37831-6283
managed by
UT-BATTELLE, LLC
for the
US DEPARTMENT OF ENERGY
under contract DE-AC05-00OR22725

CONTENTS

LIST OF FIGURES

LIST OF TABLES

1. SUMMARY

This DOE Fossil Energy project, FEAA117, addressed materials issues relevant to qualifying and deploying a Ni-base alloy for a new application in an advanced ultra-supercritical coal-fired boiler. The goal was the deployment of Haynes International alloy Haynes® 282® for applications in superheaters, reheaters, and steam delivery pipes, by completing base metal, cross-weld and all-weld metal mechanical testing needed for an ASME Boiler and Pressure Vessel Code Case and the associated microstructural analyses needed for assurance of boiler-relevant lifetimes. The alloy also is of interest for other applications including supercritical CO_2 power generation cycles. Tensile testing was completed from 20°-927°C on the three base metal alloy 282 heats, two sets of cross-weld specimens and all weld metal specimens. A total of 148 creep tests with over 565,000 h of cumulative testing was completed on base metal, cross-weld and all weld metal specimens. This project was performed with cost share from Haynes International.

2. BACKGROUND

There is a general need for research and development to bridge the gap between laboratory research and the field (i.e. for this case, the boiler and utility industry). The advanced-ultrasupercritical (A-USC) consortium [1,2] and the supercritical CO_2 (sCO_2) community [3-7] identified alloy Haynes® 282® [8-11] as an attractive alloy for the highest temperature and pressure applications in an A-USC boiler (760°C/35MPa steam) with higher creep strength than Inconel alloy 740/740H. Alloy 282 was not designed for coal ash corrosion resistance but should find application in areas without direct exposure to this environment [6,7,10,12-17]. The alloy composition is shown in Table 1 and compared to alloys in this class. The alloys with higher fractions of the strengthening γ′ phase, e.g. $Ni_3(Al,Ti)$, are more difficult to fabricate. Thus, alloy 282 creates an optimal balance between strength and fabricability. The higher strength and creep resistance of alloy 282 could translate into reduced wall thicknesses for similar steam conditions, thereby resulting in substantial cost savings for an A-USC boiler. In order for this alloy to be deployed to coal-fired boilers and other pressurized fossil energy technologies, an ASME Boiler and Pressure Vessel (B&PV) Code Case was undertaken. Testing for this code case included creep and tensile data from ~538°-927°C (1000°-1700°F) and ~22°-927°C (1700°F), respectively, on at least three commercial heats and at least one cross-weld data set. Two welding process conditions were identified for testing, gas tungsten arc welding (GTAW) and gas metal arc welding (GMAW) using a 282 filler weld wire. These specimens were made by welding two plates together and then machining specimens with the weld across the middle of the gauge section. All weld metal tests were included to assist in the process of code qualifying the 282 filler metal. All weld specimens were machined from a block of deposited 282 weld metal. The project used 24 creep frames that had been refurbished for a prior project funded under the American Recovery and Reinvestment Act in 2009 through the Advanced Manufacturing Office of the Department of Energy. Previous creep and tensile data for alloy 282 were conducted on material that used a two-step aging treatment. The A-USC boiler consortium recommended a simpler single-step aging heat treatment for alloy 282 of 4h at 800°C. Thus, none of the prior double aged data could be used for this code case.

Table 1. Nominal composition (wt.%) of alloy 282 compared to similar alloys in class including calculated γ′ fraction

Alloy	Ni	Fe	Co	Cr	Mo	Al	Ti	C	γ′
263	50	0.7*	20	20	6	0.6*	2.4*	0.06*	12
282	57	1.5*	10	19	8.5	1.5	2.1	0.06	19
740H	52	0.1	21	24.5	0.5*	1.4	1.4	0.03	~15
Réne 41	50	5*	11	19	10	1.5	3.1	0.09	24
Waspaloy	57	2*	13.5	19	4.3	1.5	3	0.08	27

* maximum value

3. APPROACH

The approach required to complete an ASME code case is relatively straightforward and in this project followed the strategy used by ORNL to generate the data for the Inconel 740 B&PV code case (ASME Code Case 2702, ASME Boiler and Pressure Vessel Code, 2012) as part of the work of the U.S. DOE – Ohio Economic Development Corporation A-USC Boiler Consortium. Haynes International's expertise in qualifying heat-resistant alloys for ASME BPV code cases was leveraged to develop a master test matrix for the creep and tensile tests. The creep tests included conditions leading to rupture times of 500 – 30,000 h at 540°-900°C. Bend and Charpy testing of a small number of specimens was conducted at Haynes International to complete the data package requirements. Standard ASME procedures including instrument calibrations were followed to ensure that all of the data are of the high quality needed for timely code case approval. While not required for the data package, a small amount of microstructural characterization was completed on selected specimens to determine if the desired microstructure of the precipitation-strengthened alloy 282 was stable over extended test times at the highest test temperatures. Mechanical properties and microstructural data for alloy 282 from the prior ORNL A-USC boiler project (completed in 2015) was used to determine the creep testing conditions and supplemented the results obtained in this project. Type S (Pt-PtRh) thermocouples were installed in 11 frames to allow the high temperature creep testing for extended times above 800°C. As part of the cost share, Haynes International provided the alloy stock, the labor to produce welded material, machined test specimens of wrought and welded Haynes 282, and the technical expertise to help guide the testing program and assemble the data package for the code case.

Haynes International supplied ~40 creep/tensile specimens of each and an example is shown in Figure 1:

- Three base metal heats of alloy 282 (2082-3-8354; 2082- 2-8389; 2082-2-8391)
  - Single age heat treatment 4h at 800°C
- Two sets of cross-weld specimens
  - Weld 1: Gas Tungsten Arc (282 filler, heat 2082-2-8391)
  - Weld 2: Gas Metal Arc (282 filler, heat 2082-3-8354)
- All weld metal 282 specimens (limited creep test matrix)

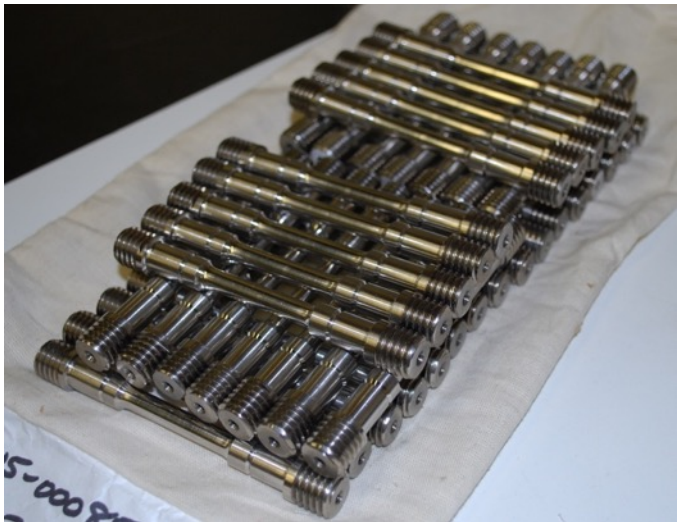

Figure 1. Alloy 282 specimens supplied by Haynes International.

4. OBJECTIVE

The primary goal of this project was to provide mechanical testing data of welded and base metal of Ni-base precipitation strengthened alloy 282 as needed for ASME BPV code qualification. Completion of an ASME code case for alloy 282 will provide a second alloy capable of achieving or exceeding 760°C steam conditions for an advanced ultra-supercritical steam coal-fired boiler.

5. MECHANICAL TESTING RESULTS

Figures 2-5 summarize the tensile data collected for this project from 22°-927°C (1700°F) in 100°F increments. The tensile test strain rate at room temperature was 0.015± 0.002/min (per ASTM standard E8-13) and at higher temperature was 0.005±0.002/min up to 2% strain and then 0.050±0.010/min (per

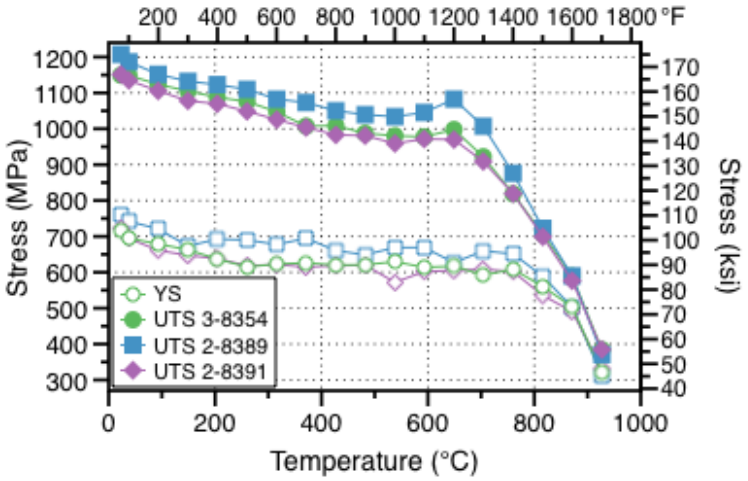

Figure 2. For three base metal heats of alloy 282, the yield stress (YS) is shown in open symbols and ultimate tensile stress (UTS) is shown in closed symbols as a function of test temperature.

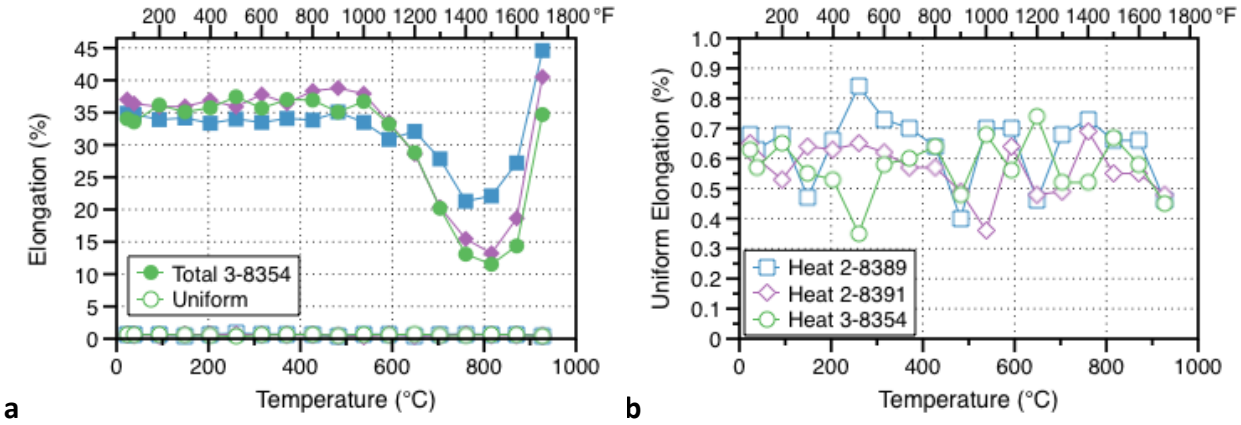

Figure 3. a) Total and uniform elongation for three base metal heats of alloy 282, the uniform elongation is shown in open symbols and the total elongation is shown in closed symbols as a function of test temperature. b) expanded y-axis to show uniform elongation data.

ASTM standard E21). Figure 2 shows the yield and ultimate tensile strength (UTS) results for the three base metal heats of alloy 282. As expected, the strength is very high up to ~700°C followed by a drop in strength at higher temperatures. Figure 3 shows the uniform and total elongation results for the three base metal heats. (Uniform elongation is the total plastic deformation at maximum load while total elongation is the elongation at fracture.) Figure 4 shows the yield and ultimate tensile strength results for the cross-weld and all weld metal specimens. For comparison, the UTS data for one base metal heat are shown as a dashed line in Figure 4 indicating that the strength values for these specimens are not significantly different from the base metal. Figure 5 shows the total elongation data for the cross-weld and all weld metal specimens. The total elongation data for the base metal heats are shown as dashed lines. Under these strain rates, the total elongation of these specimens was lower than the base metal heats. Figure 6 shows examples of cross-weld specimens indicating that failure occurred in the weld region. The tensile data are summarized in Table 2 and 3.

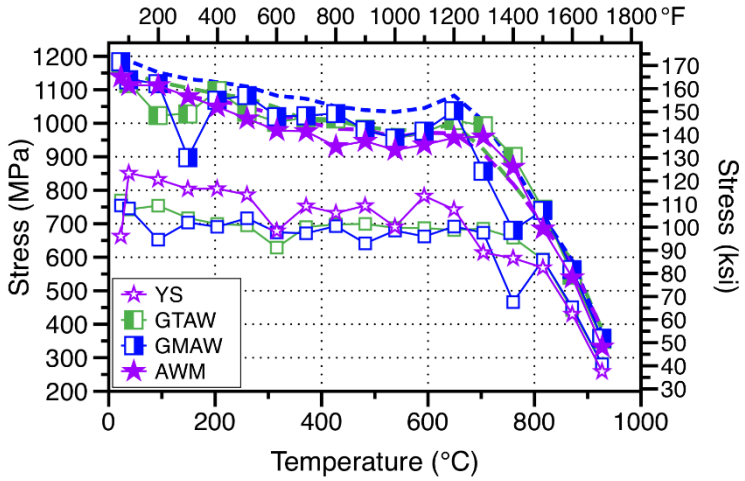

Figure 4. For cross-weld (GTAW/GMAW) and all weld metal (AWM) specimens, the yield stress (YS) is shown in open symbols and ultimate tensile stress (UTS) is shown in closed or semi-closed symbols as a function of test temperature. Base metal UTS data are shown as a dashed line.

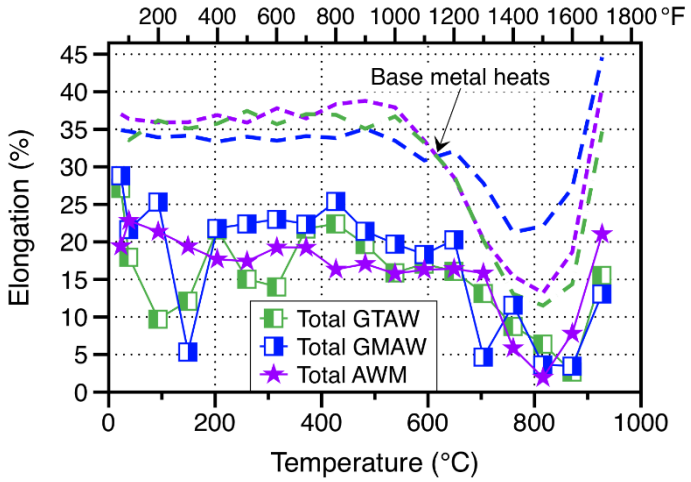

Figure 5. For cross-weld and all weld metal specimens, the total elongation is shown in closed or semi-closed symbols as a function of test temperature. Base metal total elongation data from Figure 3 are shown as dashed lines.

a  b 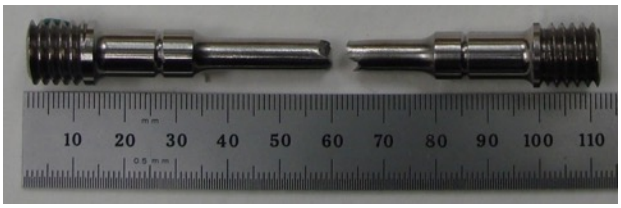

Figure 6. Images of fractured cross-weld tensile specimens (a) GTAW at 538°C and (b) GMAW at 149°C.

Table 2. Tensile data for the three base metal heats (1: 2082-3-8354; 2: 2082- 2-8389; 3: 2082-2-8391)

Temperature (°C)	YS 1 MPa	UTS 1 MPa	UE 1 %	TE 1 %	YS 2 MPa	UTS 2 MPa	UE 2 %	TE 2 %	YS 3 MPa	UTS 3 MPa	UE 3 %	TE 3 %
23	715.9	1149.4	0.63	34.0	761.1	1207.3	0.68	34.9	723.7	1151.3	0.65	37.0
38	694.9	1148.8	0.57	33.6	742.0	1186.5	0.63	34.7	694.4	1134.8	0.6	36.4
93	678.8	1123.4	0.65	36.2	720.9	1151.9	0.68	33.9	661.0	1105.5	0.53	35.9
149	662.7	1105.2	0.55	35.1	673.3	1132.2	0.47	34.2	647.2	1077.8	0.64	35.9
204	637.0	1087.5	0.53	35.8	692.4	1123.0	0.66	33.4	638.2	1069.6	0.63	36.9
260	615.0	1075.9	0.35	37.5	690.2	1109.8	0.84	34.0	618.4	1048.6	0.65	35.9
316	623.2	1047.0	0.58	35.7	677.4	1082.4	0.73	33.5	621.5	1025.4	0.62	37.8
371	626.0	1007.4	0.6	37.0	694.6	1073.1	0.7	34.1	614.6	1003.7	0.57	36.5
427	620.3	1008.5	0.64	36.9	660.5	1050.1	0.64	33.8	618.5	983.1	0.57	38.4
482	620.9	987.6	0.48	35.1	648.7	1039.3	0.4	35.1	619.9	980.8	0.49	38.8
538	629.6	980.4	0.68	36.7	668.9	1033.8	0.7	33.5	572.1	959.0	0.36	37.9
593	613.8	977.7	0.56	33.2	669.1	1045.4	0.7	30.9	602.0	971.6	0.64	33.5
649	617.3	998.0	0.74	28.8	626.9	1082.6	0.46	32.1	605.0	969.8	0.48	28.6
704	591.9	922.0	0.52	20.2	659.7	1007.1	0.68	27.8	608.9	908.9	0.49	20.4
760	608.8	818.6	0.52	13.1	651.3	876.1	0.73	21.3	601.8	819.0	0.69	15.5
816	560.3	706.5	0.67	11.5	589.0	722.5	0.66	22.1	535.3	698.8	0.55	13.2
871	503.8	589.0	0.58	14.4	502.3	590.0	0.66	27.2	491.2	576.3	0.55	18.6
927	319.8	384.2	0.45	34.7	311.8	370.8	0.46	44.6	331.3	384.6	0.48	40.5

Table 3. Tensile data for cross-weld GTAW (W1) and GMAW (W2) and all weld (AW) metal specimens

Temperature (°C)	YS W1 MPa	UTS W1 MPa	TE W1 %	YS W2 MPa	UTS W2 MPa	TE W2 %	YS AW MPa	UTS AW MPa	TE AW %
23	769.6	1176.9	27.2	754.7	1184.3	28.8	663.3	1138.8	19.4
38	742.7	1119.1	18.0	745.8	1130.4	21.7	851.3	1113.4	22.8
93	754.1	1023.6	9.7	652.5	1118.7	25.3	832.7	1112.6	21.4
149	717.0	1028.5	12.1	703.5	898.0	5.4	804.1	1080.2	19.4
204	699.4	1098.0	21.6	690.8	1069.2	21.8	804.9	1049.2	17.7
260	695.1	1033.6	15.1	716.5	1083.3	22.4	786.7	1013.6	17.4
316	628.8	1003.6	14.0	674.1	1020.2	23.0	678.9	978.8	19.3
371	690.4	1017.2	21.7	671.5	1022.9	22.4	753.1	975.7	19.3
427	698.2	1013.7	22.4	693.1	1029.2	25.4	732.0	930.8	16.3
482	699.5	983.0	19.7	641.5	980.4	21.4	754.1	946.6	17.1
538	687.8	955.3	15.9	679.7	956.2	19.7	690.9	920.1	15.8
593	687.0	972.4	17.1	662.0	977.0	18.3	782.8	935.9	16.3
649	681.1	1008.4	16.1	691.9	1038.0	20.3	742.7	956.6	16.4
704	685.4	992.8	13.1	673.0	857.3	4.7	613.8	959.5	15.8
760	658.4	901.6	8.8	466.3	680.9	11.6	597.2	869.2	5.9
816	593.2	744.1	6.4	592.3	740.3	3.6	568.9	684.7	1.9
871	442.8	546.6	2.7	450.7	563.9	3.5	430.2	539.0	7.8
927	281.2	355.3	15.6	280.6	358.5	13.1	259.1	332.3	21.1

The creep data are summarized in Tables 4 and 5 for the base metal heats, cross-weld and all weld metal specimens, respectively. Figure 7 plots the data using the Larson Miller parameter. The cross-weld data are not significantly different from the base metal results. After failure, the specimens were analyzed to determine the elongation and reduction in area. Example values for the three heats are shown in Figures 8a and 8b as a function of test temperature. For the majority of tests, extensometers were used to measure strain. Minimum creep rates (MCRs) could be calculated from each experiment. The MCRs are shown in Figure 8d as a function of stress. Most of the MCRs were founded to be located within a range of between 3.0E-5 to 3.0E-3 %/h. The exponent n for a power-law curve fit at each temperature is shown. The stress exponents varied but tended to decrease with increasing testing temperature. Further creep data analysis is shown in Section 7.

Table 4. Summary of creep testing results for the base metal heats including the calculated minimum creep rate (MCR) and measured reduction in area (RA)

Heat	Expected Life (h)	Stress (MPa)	Temperature (°C)	Rupture Time (h)	MCR (%/h)	Final strain (%)	Elongation (%)	RA (%)
1	500	806	593	123.7	9.64E-04	4.28	12.75	12.58
1	1400	749	593	665.6	2.08E-04	0.32	7.43	8.8
1	4000	693	593	5136.1	–	–	2.97	4.16
1	10000	637	593	13133.3	–	–	0.46	2.4
1	500	695	621	908	–	–	4.38	2.98
1	4000	584	621	7136.2	–	–	–	–
1	500	633	649	694	2.69E-04	0.38	0.85	2.78
1	1400	578	649	1498.9	3.04E-04	0.59	2.54	2.98
1	4000	520	649	2009.2	8.00E-05	0.45	2.31	0.2
1	10000	469	649	5845.6	8.10E-05	1.69	2.66	3.57
1	500	548	677	787.8	–	–	3.05	3.76
1	4000	442	677	2674.2	2.27E-04	7.99	8.02	9.75
1	500	479	704	452.5	1.18E-03	6.06	6.83	9.38
1	1400	425	704	1286.6	9.48E-04	14.04	15.07	19.36
1	1400	424	704	1626.3	6.67E-04	25.96	29.01	32.77
1	4000	372	704	3403.4	7.80E-05	1.77	23.57	29.38
1	10000	331	704	7844.9	9.10E-05	17.06	16.35	23.79
1	500	405	732	653.6	1.36E-03	1.96	15.2	20.94
1	500	303	732	4344.3	1.77E-04	21.83	21.97	27.66
1	500	336	760	572.7	1.61E-03	20.12	25.09	35.91
1	1400	288	760	1807.9	6.72E-04	20.92	12.76	14.89
1	4000	241	760	4915.1	1.27E-04	25.95	23.67	40.52
1	10000	201	760	11079.6	7.80E-05	27.04	27.59	43.69
1	500	274	788	659.1	1.85E-03	29.22	29.93	37.74
1	4000	183	788	5050	2.41E-04	30.78	34.5	41.63
1	500	212	816	687.7	1.20E-03	25.88	27.15	42.55
1	1400	169	816	1760.6	7.39E-04	27.07	28.5	43.31
1	4000	132	816	5058.3	2.07E-04	29.54	29.9	33.21
1	10000	101	816	16914	–	–	17.68	17.21
1	500	166	843	440.4	2.08E-03	30.78	–	–
1	4000	93	843	6170.7	2.47E-04	32.02	–	–
1	500	114	871	651.3	1.26E-03	24.53	29.15	38.61
1	1400	88	871	1889.6	1.05E-03	31.2	–	–
1	1400	84	871	4172.7	3.08E-04	30.58	31.92	38.85
1	10000	46	871	17794.7	1.72E-04	13.72	14.94	14.26

Heat	Expected Life (h)	Stress (MPa)	Temperature (°C)	Rupture Time (h)	MCR (%/h)	Final strain (%)	Elongation (%)	RA (%)
1	500	83	899	682.3	1.62E-03	31.21	31.53	35.69
1	4000	43	899	7485.4	3.02E-04	17.04	19.42	17.07
1	500	54	927	1187.2	2.07E-03	32.93	20.37	33.44
1	1400	41	927	3048.5	1.00E-03	21.15	21.55	18.18
1	4000	32	927	5686.2	5.75E-04	27	–	–
1	10000	26	927	9376.4	9.40E-05	37.72	24.74	18.63
2	500	775	593	1505.1	–	–	3.78	6.55
2	1400	738	593	4231.5	6.80E-05	0.56	–	–
2	4000	682	593	13978.6	–	–	4.2	2.19
2	10000	624	593	19923.8	1.20E-05	0.98	1.76	6.91
2	500	617	649	993.9	–	–	5.17	5.17
2	1400	570	649	1796.9	3.39E-04	4.46	6	5.91
2	4000	519	649	3498.4	–	–	9.52	8.4
2	10000	474	649	6825.5	1.32E-04	11.86	13.26	12.93
2	500	474	704	493.3	–	–	21.47	25.99
2	500	478	704	507.9	2.43E-03	20.64	16.75	28.2
2	4000	373	704	2946.4	–	–	35.04	38.84
2	10000	329	704	6522.2	2.05E-04	11.37	32.71	42.71
2	500	339	760	495.8	–	–	–	–
2	1400	290	760	1266.3	–	–	35.49	58.9
2	4000	241	760	3594.5	–	–	34.19	56.1
2	10000	201	760	7992.6	1.20E-04	22.18	46.61	50.36
2	30000	158	760	25306.3	–	–	–	–
2	500	217	816	428	–	–	–	–
2	1400	173	816	855.3	9.49E-04	40.5	41.25	57
2	4000	132	816	3713.9	–	–	42.68	53.22
2	10000	103	816	7911.7	1.00E-04	31.13	36.5	42.55
2	500	117	871	388	–	–	–	–
2	1400	89	871	1511.4	1.25E-03	31.04	42.64	45.39
2	4000	63	871	3760.6	1.70E-04	31.17	45.36	46.16
2	10000	46	871	7871.9	1.25E-04	18.6	21.43	25.17
2	500	55	927	474.2	–	–	47.59	42.09
2	1400	42	927	1240.9	1.01E-03	13.6	38.43	38.87
2	4000	32	927	2757.4	4.20E-04	30.44	33.49	39.86
2	10000	26	927	4747.6	1.17E-04	38.56	42.12	37.57
3	500	798	593	128.7	4.13E-04	0.52	11.11	9.01
3	1400	738	593	328.8	–	–	8.02	6.16
3	4000	676	593	2179.6	–	–	3.96	1.61
3	10000	637	593	10556.2	–	–	–	–
3	500	627	649	315.1	2.83E-04	0.19	4.21	2.19
3	1400	574	649	618.1	–	–	2.33	3.38
3	4000	514	649	1982.9	1.51E-04	0.57	3.63	1.23
3	10000	466	649	4898.8	3.50E-05	1.32	2.88	0
3	5000	475	704	412	4.80E-04	3.3	5.6	3.58
3	1400	424	704	758.1	–	–	8.61	7.1
3	4000	368	704	3258	–	–	18.18	21.27
3	4000	365	704	3259.1	–	–	18.29	18.71
3	10000	323	704	8508.4	1.50E-04	18.22	18.5	28.6
3	500	337	760	550	2.52E-03	20.72	18.17	16.6
3	1400	289	760	619.2	–	–	22.82	30.61

Heat	Expected Life (h)	Stress (MPa)	Temperature (°C)	Rupture Time (h)	MCR (%/h)	Final strain (%)	Elongation (%)	RA (%)
3	4000	239	760	5111.1	–	–	24.8	39.6
3	10000	199	760	12005	–	–	29.95	48.76
3	500	218	816	751.8	8.25E-04	28.37	32.02	25.98
3	1400	173	816	2081.7	–	–	34.84	40.28
3	4000	132	816	3597.4	–	–	–	–
3	10000	102	816	14634.9	–	–	–	–
3	500	125	871	472.5	–	–	40.86	46.52
3	1400	92	871	1967.4	–	–	–	–
3	4000	63	871	8650.9	–	–	31.32	34.31
3	10000	48	871	20251.3	–	–	–	–
3	500	59	927	1018.9	2.27E-03	40.94	95.66	39.75
3	500	59	927	1551.3	–	–	30.14	16.2
3	1400	44	927	2706.1	–	–	35.68	30.57
3	4000	42	927	3585.5	2.88E-04	31.88	35.93	30.79
3	10000	25	927	14555.1	–	–	–	–
1*	15000	443	649	2062	–	–	–	–
2*	15000	443	649	2062	–	–	–	–
2*	15000	303	704	2158	–	–	–	–
2*	15000	94	816	1990	–	–	–	–
2*	15000	45	871	1990	–	–	–	–
2*	15000	23	927	1990	–	–	–	–
3*	15000	443	649	2062	–	–	–	–
3*	15000	303	704	2158	–	–	–	–

*Ongoing

Table 5. Summary of creep testing results for the cross-weld GTAW (W1) and GMAW (W2) and all weld metal (AWM) specimens

Heat	Expected Life (h)	Stress (MPa)	Temperature (°C)	Rupture Time (h)	Elongation (%)	RA (%)
AWM	1000	745	593	452	3.6	3.56
AWM	4500	659	593	6085.2	–	–
AWM	1000	383	704	1647.3	–	–
AWM	4500	362	704	1962.7	1.68	1.21
AWM	1000	165	816	549.6	0.65	1.21
AWM	4500	130	816	2220	6.5	2.39
AWM	1000	43	927	1345.5	–	–
AWM	4500	31	927	3783.3	–	–
W1	1000	758	593	644.9	3.74	2.21
W1	2500	693	593	4100.1	–	–
W1	4500	674	593	2098.7	3.95	0.16
W1	6000	644	593	8532.3	–	–
W1	1000	439	704	353.8	2.57	0.2
W1	4500	364	704	1872	–	–
W1	6000	348	704	2869	4.57	2.19
W1	2500	342	704	2105.5	–	–

Heat	Expected Life (h)	Stress (MPa)	Temperature (°C)	Rupture Time (h)	Elongation (%)	RA (%)
W1	1000	188	816	644.5	8.31	3.19
W1	2500	133	816	2490.4	–	–
W1	4500	128	816	2850.5	–	–
W1	6000	120	816	3374.2	1.92	4.96
W1	1000	43	927	1696.1	–	–
W1	2500	37	927	3301.7	11.49	9.38
W1	4500	30	927	4628	–	–
W1	6000	28	927	5568	7.48	1.59
W2	1000	745	593	2321.9	–	–
W2	2500	706	593	3994.9	2.84	3.39
W2	4500	659	593	9666	–	–
W2	6000	658	593	7856	3.02	1.41
W2	2500	388	704	786	1.3	0.6
W2	1000	383	704	1218.5	–	–
W2	4500	360	704	991.9	2.56	1.4
W2	6000	348	704	1794.7	2.98	1.4
W2	1000	165	816	620.1	0.84	1.01
W2	2500	133	816	1869.8	–	–
W2	4500	130	816	2247	4.28	6.54
W2	6000	119	816	3305.7	5.25	2.01
W2	1000	43	927	1048.9	–	–
W2	2500	32	927	3090	–	–
W2	4500	30	927	3069	–	–
W2	6000	28	927	5874.8	–	–

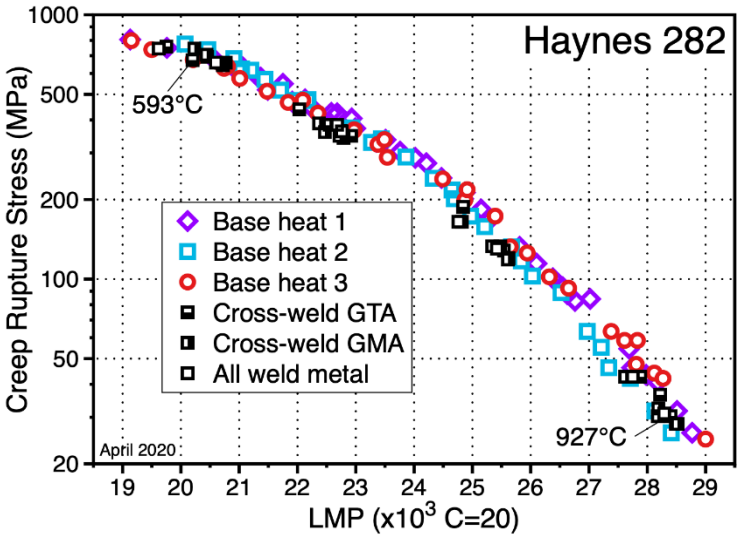

Figure 7. Larson-Miller parameter plot of the creep data.

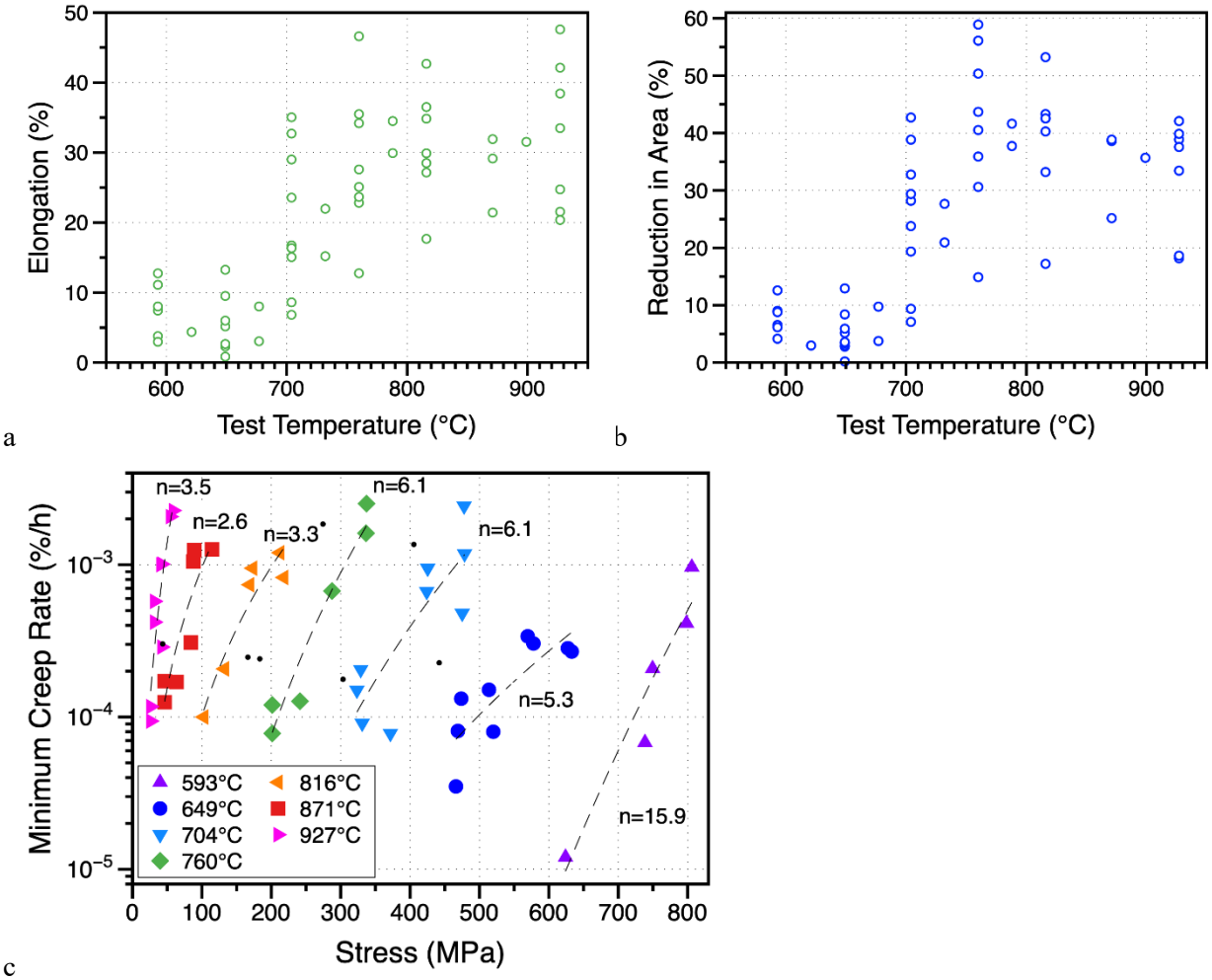

Figure 8. Additional analyses performed on the base metal creep data: (a) elongation, (b) reduction in area and (c) minimum creep rate.

6. POST EXPOSURE CHARACTERIZATION

Basic microstructural characterization was performed on selected creep tested specimens listed in Table 6 covering four of the highest testing temperatures (816, 871, 899 and 927 °C). All the specimens ruptured with mainly an intergranular failure mode. In general, the stress influenced γ' morphology (shape and size) and accelerated the microstructural changes.

Figure 9 shows light microscopy images of polished cross-sections of the ruptured 282 specimens after failure at 816°C (Fig. 9a), 871°C (Fig. 9b) and 927°C (Fig. 9c) and multiple stresses based on the test matrix. The cavity density and location varied with stress and temperature. For example, at 871°C, a higher density of cavities was observed at a greater depth for a stress of 92 MPa compared to 46 MPa where more localized near surface cavities and cracks were observed. Specimens tested at 927°C showed the presence of cavities and cracks throughout the entire gauge section for all stresses with a higher density than at lower temperatures. Microstructural changes were observed at 871°C and higher.

Table 6. Summary of selected creep tested specimens used for microstructural characterization

Heat	Target Life	MPa	°C	Hours	MCR(%/h)	Fstrain (%)
3	4000	42	927	3585.5	2.88E-04	31.88
2	10000	26	927	4747.6	1.17E-04	38.56
1	10000	26	927	9376.4	9.40E-05	37.72
3	10000	25	927	14555		
1	4000	43	899	7485.4	3.02E-04	17.04
3	1400	92	871	1967.4		
3	4000	63	871	8650.9		
2	10000	46	871	7871.9	1.25E-04	18.6
1	10000	46	871	**17795**	1.72E-04	13.72
1	10000	100	816	16914		
3	10000	101	816	14182		
2	10000	102	816	7911.7		

Figure 10 shows examples of the 282 microstructure from the gauge (Fig. 10a) and grip (Fig. 10b) section after rupture at three different stress levels at 816°C. In the gauge section, grain boundary γ' depletion zones (bright regions without precipitates) were observed, whereas this depletion was not apparent in the low-stress (grip) region. In the gauge sections, cavities and cracks were found to be present along alloy grain boundaries. As expected, internal oxidation was observed in the material exposed by cracks and cavities. The oxidation resulted in enhanced local γ' depletion as Al and Ti are consumed by internal oxidation. Further characterization using SEM is needed to investigate these microstructural changes at higher magnification.

Figure 11 shows light microscopy images of the microstructure along the surface of the gauge section for three similar stress levels at 816°C. The γ' phase depletion depth increased with the testing time. Internal oxidation as well as crack propagation along alloy grain boundaries also increased with time. Within the γ' phase depletion zone, precipitate formation was observed which is most likely η phase (Ni_3Ti). After 7,911.7 h at 102 MPa, the precipitates were random and ~8μm. The number and size increased at longer times. The η phase is known to be brittle with little strain tolerance [18] and may weaken the structure since η is non-coherent with the matrix.

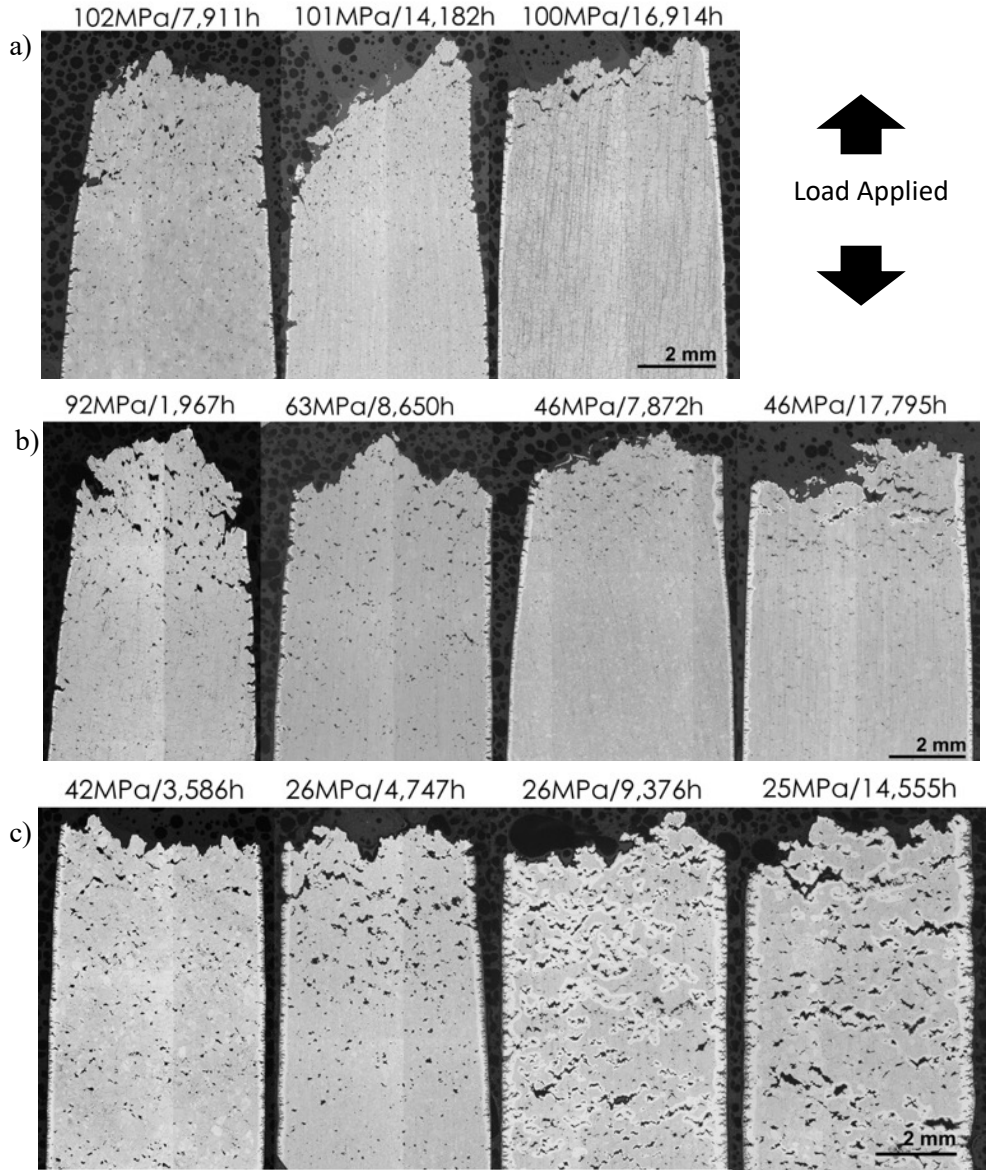

Figure 9. Light microscopy images showing polished cross-section of the creep rupture base metal 282 specimens after a failure for three different temperatures at (a) 816°C, b) 871°C and c) 927°C.

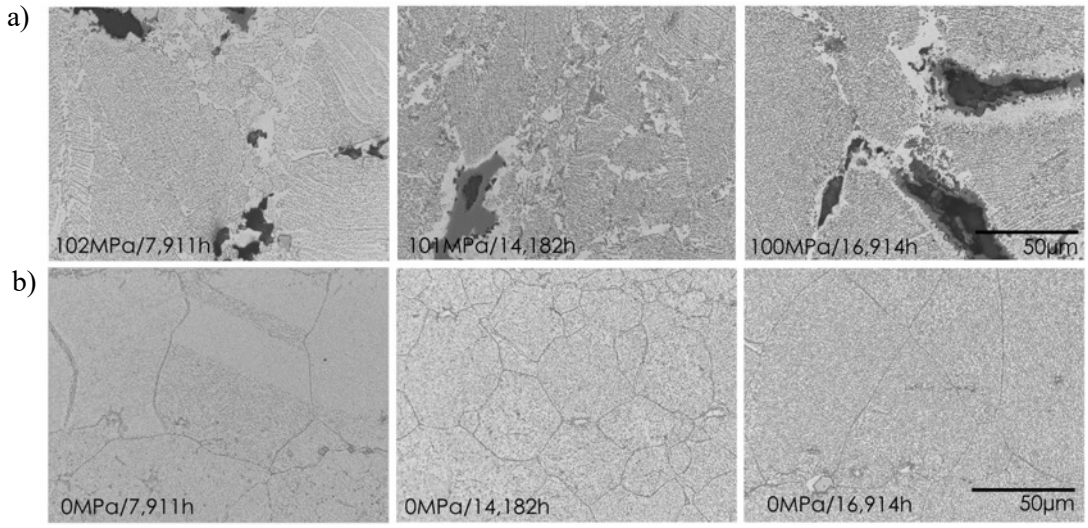

Figure 10. Higher magnification light microscopy images showing microstructure from the gauge (a) and grip (b) section after the creep rupture of base metal 282 specimens for various stress levels tested at 816°C.

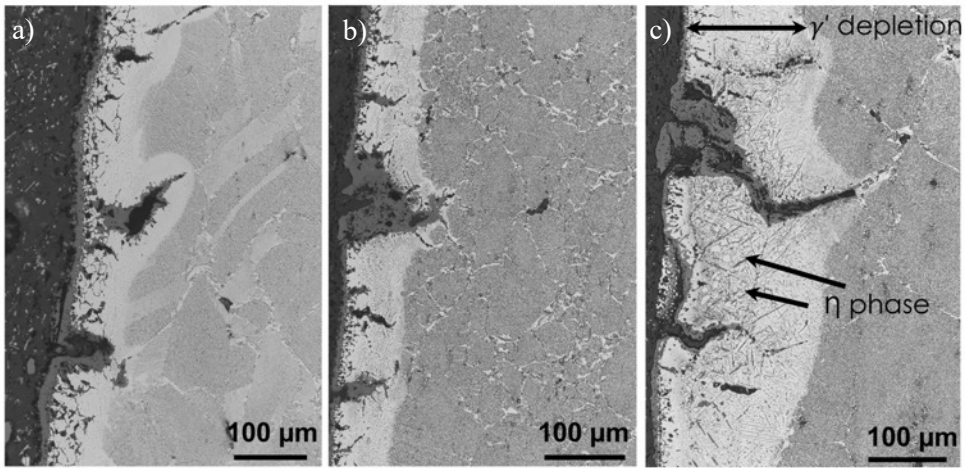

Figure 11. Light microscopy images showing microstructure along edge of the gauge section after the creep rupture of base metal 282 specimens at 816°C (a) 102MPa for 7911.7 h, (b) 101MPa for 14182 h and (c) 100MPa for 16914 h.

Figure 12 shows BSE-SEM images with EDS elemental maps showing the microstructure at the surface of the gauge section after rupture at 871°C for 1967 h (92 MPa) and 17,795 h (46 MPa). Randomly oriented η phase (Ni_3Ti) within the γ' phase depleted region was observed after the shorter exposure in Figure 12a, whereas larger platelets of η phase within the depleted zone were clearly visible after 17,795 h. EDS analysis confirmed that the platelets were enriched in Ti. The oxide formed on the surface and within the cracks is mainly Cr-rich with the outermost surface layer enriched in Ti. The internal oxidation is rich in Al.

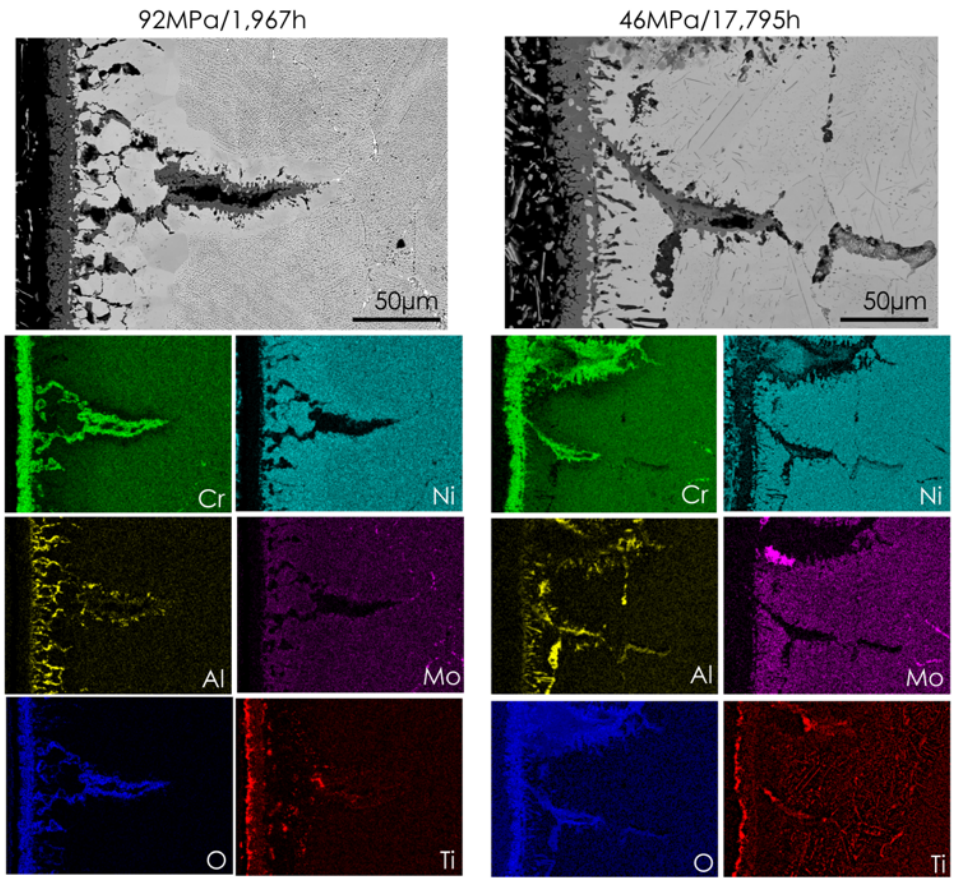

Figure 12. BSE-SEM images with EDS elemental maps showing microstructure within the gauge section along the edge of the sample after the creep rupture of base metal 282 specimens tested at 92MPa for 1,967h (a) and at 46MPa for 17,795h (b) at 871°C.

Figure 13 shows BSE-SEM images of the microstructure within the gauge section after creep rupture of 282 specimens tested at 927°C with applied stress of 42 MPa and 25 MPa resulting in lifetimes of 3,586 h and 14,555h, respectively. Coarsening of γ' phase was observed. Also, large η phase (Ni_3Ti) was observed particularly in the longer exposure time. TEM is needed to confirm the η phase formation. Figure 14 shows the surface of the gauge section after testing at 927°C. Significant γ' phase depletion was observed at the surface as well as internal oxidation and crack propagation. After 14,555 h, a high volume of large platelets of the η phase was found within the γ' phase depletion zone. Precipitation of η phase (Ni_3Ti) is most likely due to the Ti content exceeding the solubility limit within the alloy matrix. The internal oxidation is mainly associated with Al. The oxide formed on the surface and within the cracks is Cr-rich with Ti enrichment. It is not surprising that the oxidation and microstructural changes were high at 927°C. In actual applications, this alloy might be coated to prevent this attack.

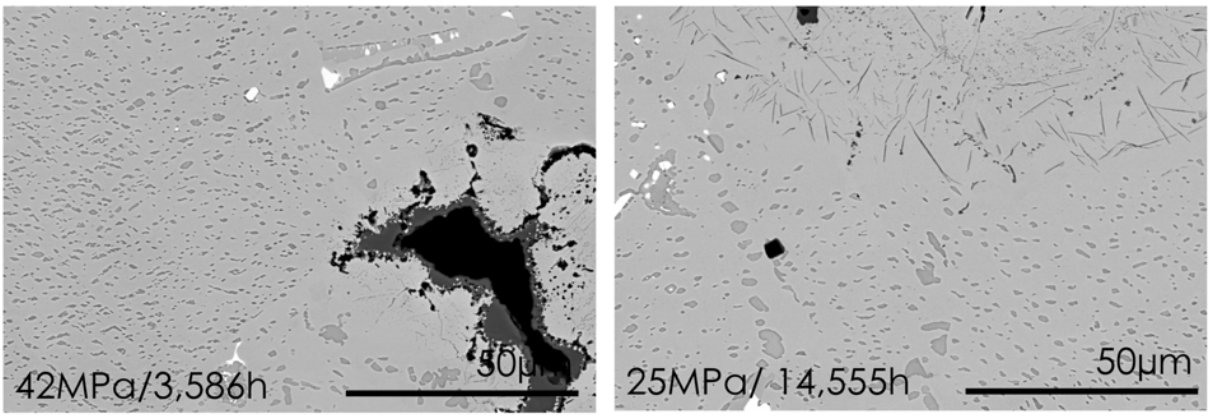

Figure 13. BSE-SEM images showing microstructure within the gauge section of base metal 282 specimens tested at 927°C for (a) 3,586 h at 42 MPa and (b) 14,555 h at 25MPa.

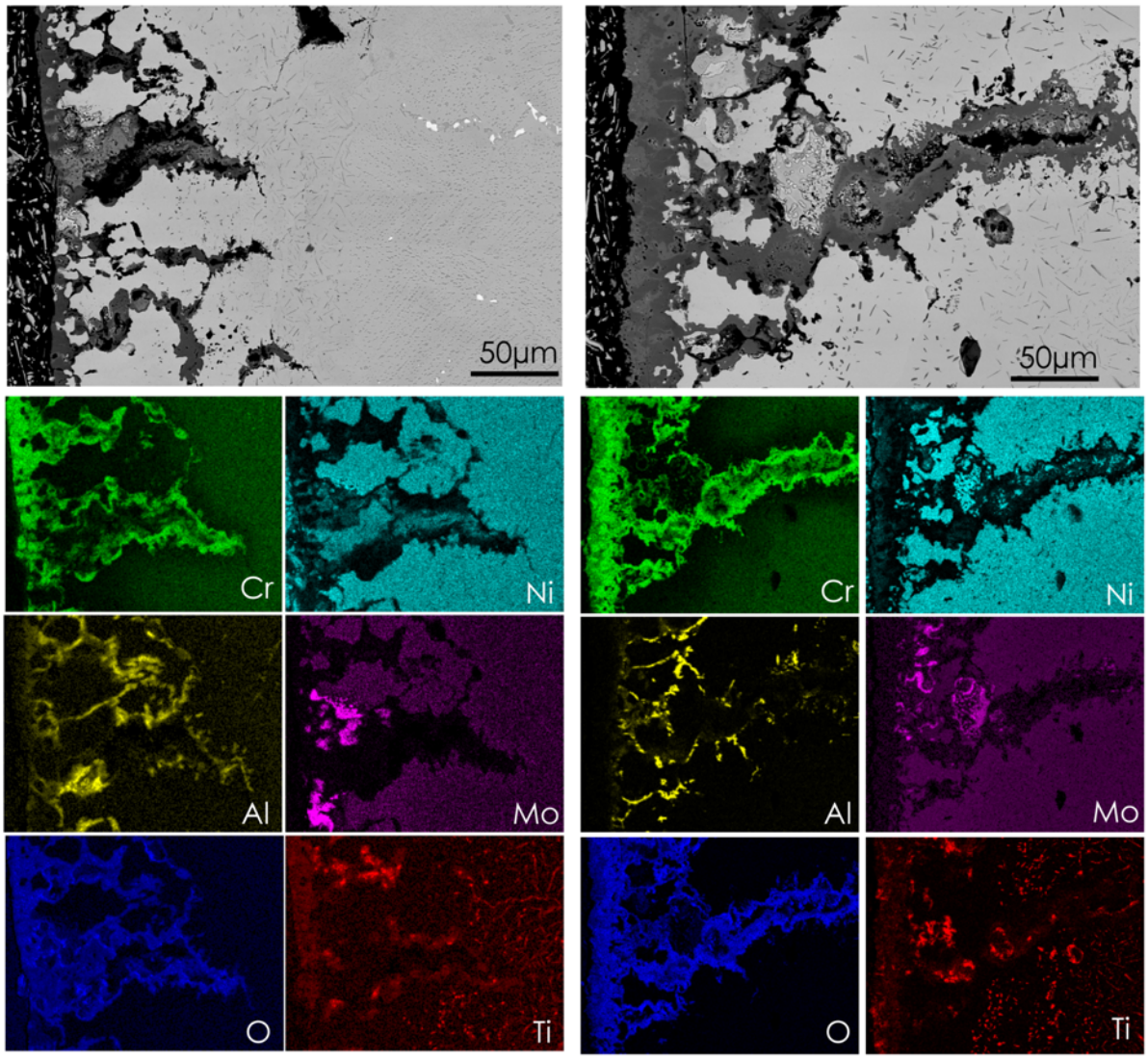

Figure 14. BSE-SEM images with EDS elemental maps showing the surface of the gage section of base metal 282 specimens tested at 927°C for (a) 3,586 h at 42 MPa and (b) 14,555 h at 25MPa.

7. CREEP DATA ANALYSIS

Time to rupture data resulting from the creep tests of single-aged base metal specimens are shown in Figure 15. On- going tests at the time of writing this report are shown by the data points with horizontal arrows. Figure 15 shows that the tensile creep behavior of single aged wrought H282 is almost time independent (i.e., very little creep occurring) up to 621 °C. Creep also appears to be very low at 649 °C.

Figure 16 is a Monkman-Grant plot (minimum creep rate vs. lifetime) of all the test data; it is clear that the data do not have a well-correlated linear relationship on a log-log plot. Specimens at the two lowest temperatures, 593 and 649 °C, failed up to an order of magnitude faster than those at higher temperatures with similar minimum creep rates. Figure 17 shows that the data scatter in Figure 16 does not appear to be influenced by the three (3) different heats; i.e., there is no obvious heat to heat variation in life vs minimum creep rate. As shown in Figure 18, after removing the 593 and 649°C data points, the remainder of the data have a much tighter linear correlation, other than two data points at 704 °C that appear lower than the bulk of the data.

A modified form of the Monkman – Grant equation that includes the strain at failure has been shown by other researchers to provide a better fit of the data [19]. Figure 19 shows a modified Monkman-Grant plot where time to rupture is divided by strain at failure. This produced a better correlation of data at all temperatures, but a disconnect between two linear segments can be seen where time divided by strain is about 100,000.

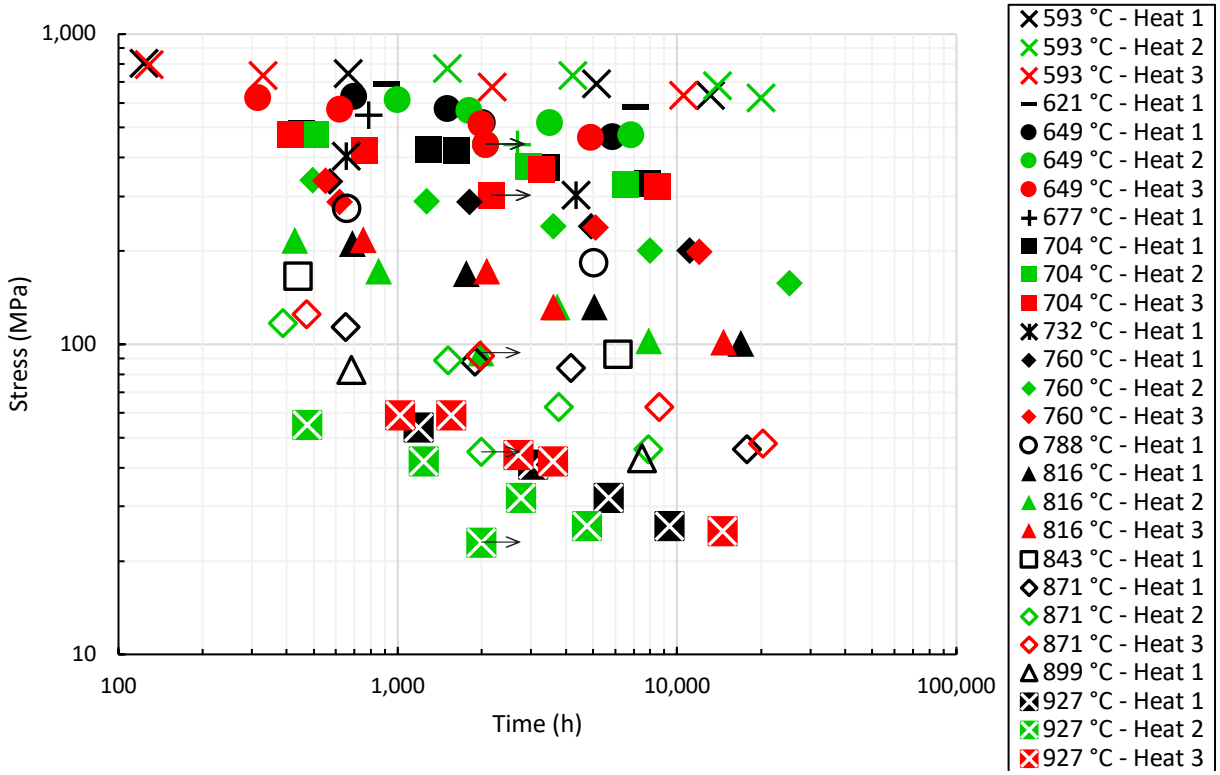

Figure 15. Plot of applied stress versus creep life of single-aged 282 base metal specimens at temperatures from 593 to 927 °C. Test temperatures are differentiated by symbol and heats are differentiated by color.

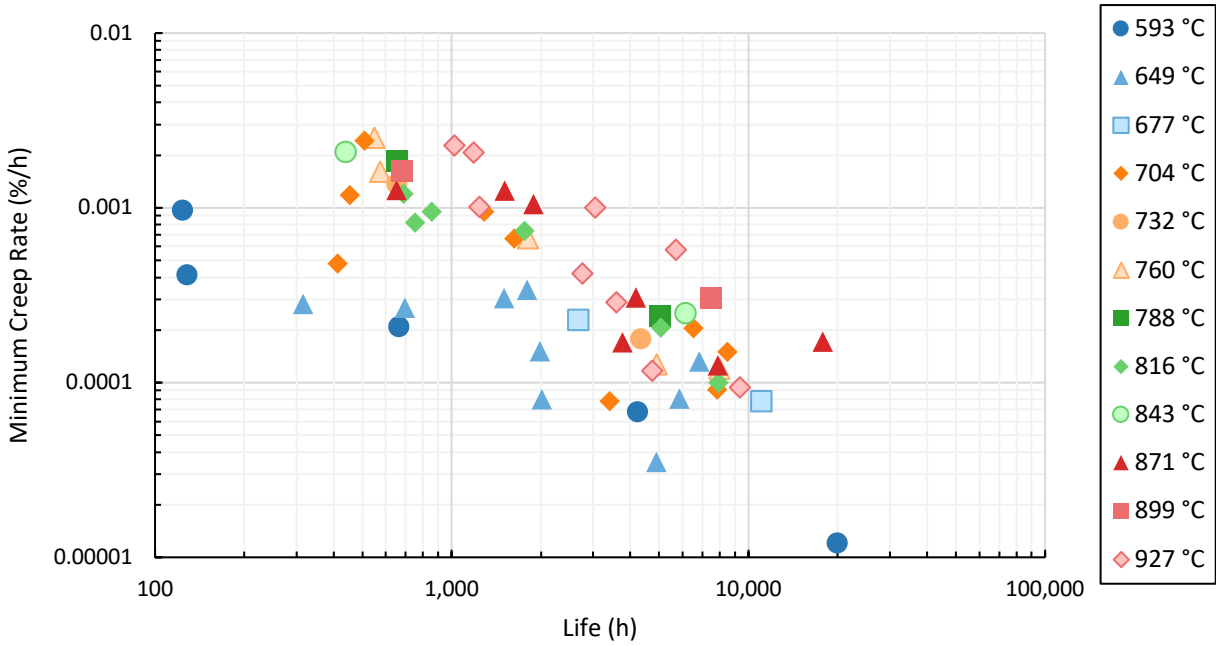

Figure 16. Monkman-Grant plot (minimum creep rate versus life) of single-aged 282 base metal specimens at temperatures from 593 to 927 °C.

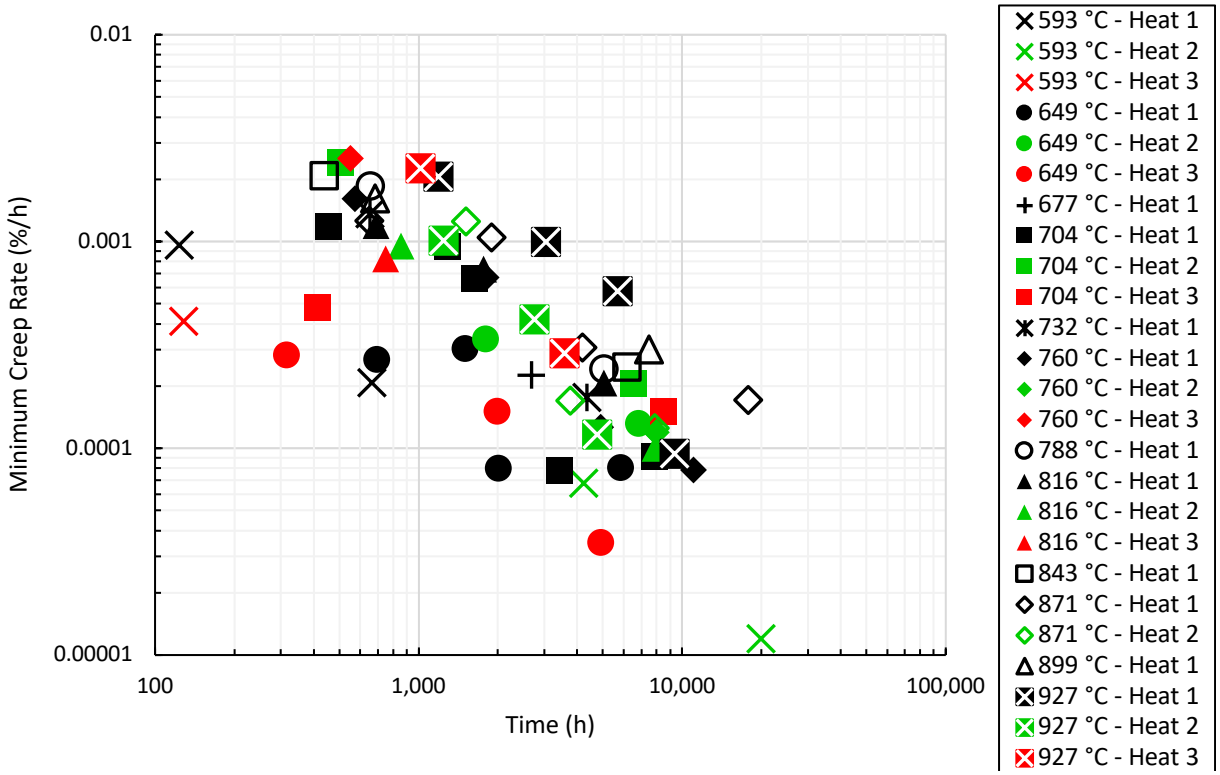

Figure 17. Monkman-Grant plot (minimum creep rate versus life) of single-aged 282 base metal specimens at temperatures from 593 to 927 °C. Test temperatures are differentiated by symbol and heats are differentiated by color.

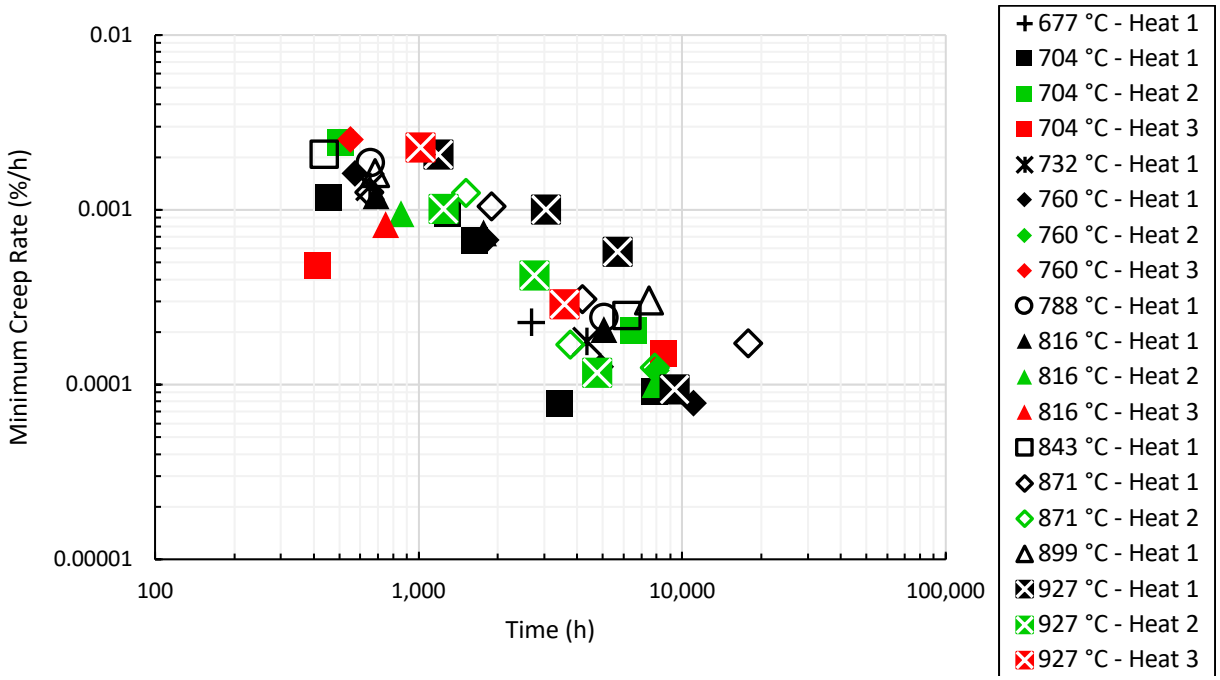

Figure 18. Monkman-Grant plot (minimum creep rate versus life) of single-aged 282 base metal specimens at temperatures from 677 to 927 °C. Test temperatures are differentiated by symbol and heats are differentiated by color.

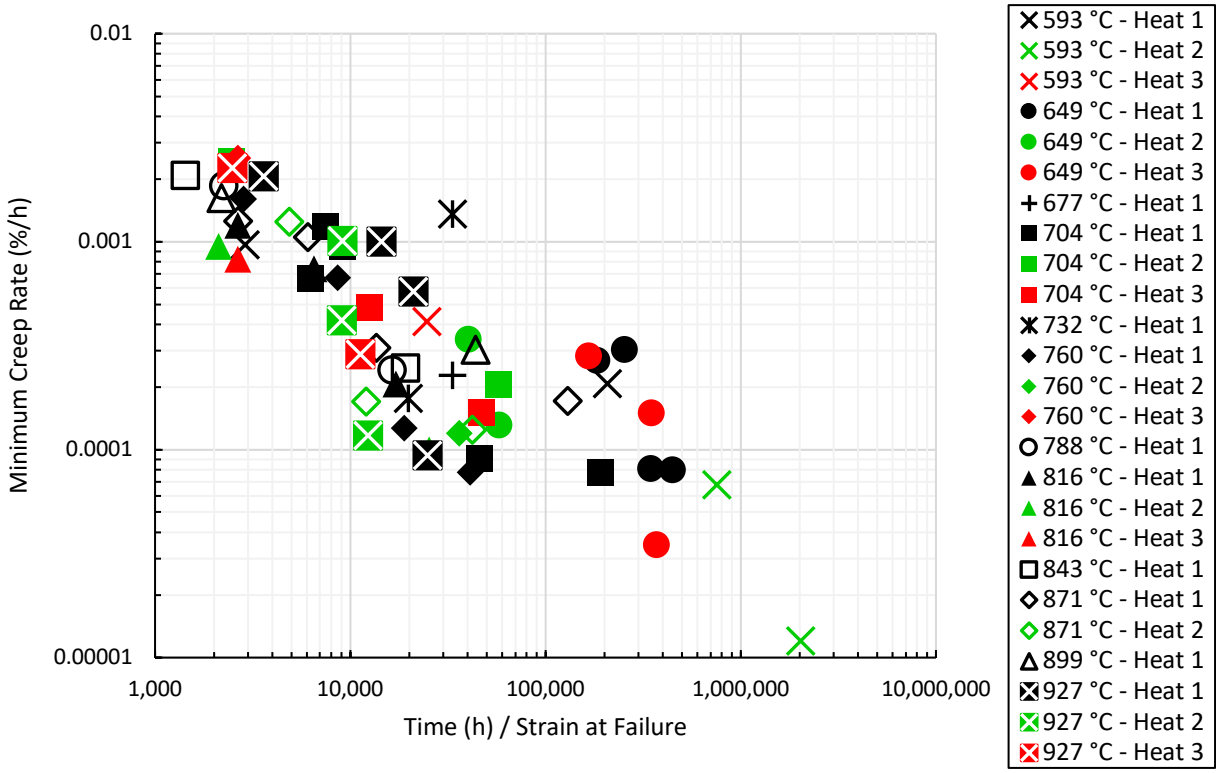

Figure 19. Modified Monkman-Grant plot (minimum creep rate versus life divided by strain at failure) of single-aged 282 base metal specimens at temperatures from 593 to 927 °C. Test temperatures are differentiated by symbol and heats are differentiated by color.

8. ACKNOWLEDGMENTS

This research was supported by the US Department of Energy, Office of Fossil Energy, Crosscutting Technology Program, award number FEAA117. The authors would like to thank Tracie Lowe and Tom Geer for assistance with the characterization, Mark Render (National Energy Technology Laboratory) for preparation of Figures 15 through 19 and assistance with formatting the data tables. A special thanks to project monitor Vito Cedro (National Energy Technology Laboratory) for his input into the report and his guidance during the project.

9. REFERENCES

1. R. Viswanathan, J. F. Henry, J. Tanzosh, G. Stanko, J. Shingledecker, B. Vitalis, and R. Purgert, "U.S. Program on Materials Technology for Ultra-Supercritical Coal Power Plants," *J. Mater. Eng. Performance* **14**(3) (2005) 281-285.
2. R. Viswanathan, J. Shingledecker, and R. Purgert, "Evaluating Materials Technology for Advanced Ultrasupercritical Coal-Fired Plants," *Power* **154**(8) (2010) 41-45.
3. R. J. Allam, M. R. Palmer, G. W. Brown Jr., J. Fetvedt, D. Freed, H. Nomoto, M. Itoh, N. Okita, and C. Jones Jr., "High efficiency and low cost of electricity generation from fossil fuels while eliminating atmospheric emissions, including carbon dioxide," *Energy Procedia* **37**, (2013) 1135.
4. I. G. Wright, B. A. Pint, J. P. Shingledecker, and D. Thimsen, "Materials Considerations for Supercritical CO_2 Turbine Cycles," ASME Paper #GT2013-94941, presented at the International Gas Turbine & Aeroengine Congress & Exhibition, San Antonio, TX, June 3-7, 2013.
5. B. A. Pint, "Performance of Wrought Superalloys in Extreme Environments," in E. Ott et al. (Eds.), *Proceedings of the 9th International Symposium on Superalloy 718 and Derivatives*, TMS, Warrendale, PA, 2018, pp.165-178.
6. B. A. Pint and J. R. Keiser, "Effect of Pressure and Thermal Cycling on Long-Term Oxidation in Supercritical CO_2," NACE Paper C2019-12750, Houston, TX, presented at NACE Corrosion 2019, Nashville, TN, March 2019.
7. V. P. Deodeshmukh and B. A. Pint, "Long-Term Performance of High Temperature Alloys in Oxidizing Environments and Supercritical CO_2," in *Proceedings of the Joint EPRI – 123HiMAT International Conference on Advances in High Temperature Materials*, J. Shingledecker and M. Takeyama eds., ASM International, Materials Park, OH, 2020, pp. 953-966.
8. L. M. Pike, "HAYNES® 282® alloy - A new wrought superalloy designed for improved creep strength and fabricability," Proceedings of the ASME Turbo Expo, ASME, New York, 2006, Vol.4 pp.1031-1039.
9. L. M. Pike, "Development of a Fabricable Gamma-Prime (γ') Strengthened Superalloy," in *Superalloys 2008*, R. C. Reed et al. eds TMS, Warrendale, PA, 2008, pp.191-200.
10. L. M. Pike and S. K. Srivastava, "Oxidation Behavior of Wrought Gamma-Prime Strengthened Alloys," Materials Science Forum 595-598 (2008) 661-671.
11. J. A. Hawk, T. L. Cheng, J. S. Sears, P. D. Jablonski, and Y. H. Wen, "Gamma Prime Stability in Haynes 282: Theoretical and Experimental Considerations," *J. Mater. Eng. Performance* **24** (2015) 4171-4181.
12. E. Essuman, L. R. Walker, P. J. Maziasz, and B. A. Pint, "Oxidation Behavior of Cast Ni-Cr Alloys in Steam at 800°C," *Mater Sci Technol* **29** (2013) 822-827.
13. A. Shyam, C. S. Hawkins, R. Shibayan, S. Dryepondt, D. L. Erdman III, and P. J. Maziasz, "The Effect of Steam on the Elevated Temperature High Cycle Fatigue Life of Haynes 282® Superalloy," in Proc. 10th Liege Conference on Materials for Advanced Power Engineering, Liege, Belgium, September 2014.

14. F. A. Pérez-González, N. F. Garza-Montes-de Oca, and R. Colás, "High Temperature Oxidation of the Haynes 282© Nickel-Based Superalloy," *Oxid Met* **82** (2014) 145-161.
15. V. Deodeshmukh and B. A. Pint, (2016) "Fireside Corrosion and Steamside Oxidation Behavior of HAYNES 282 Alloy for A-USC Applications," in Proc. 8th Inter. Conf. on Advances in Materials Technology for Fossil Power Plants, ASM International, Materials Park, OH, 2016, pp.913-924.
16. T. Dudziak, V. Deodeshmukh, L. Backert, N. Sobczak, M. Witkowska, W. Ratuszek, K. Chrusciel, A. Zielinski, J. Sobczak, and G. Bruzda, "Phase Investigations Under Steam Oxidation Process at 800°C for 1000 h of Advanced Steels and Ni-Based Alloys," *Oxid. Met.* **87** (2017) 139-158.
17. R. I. Olivares, D. J. Young, T. D. Nguyen, and P. Marvig, "Resistance of High-Nickel, Heat-Resisting Alloys to Air and to Supercritical CO_2 at High Temperatures," *Oxid. Met.* **90** (2018) 1-25.
18. Superalloys II. Edited by C.T. Sims, N.S. Stoloff and W.C. Hagel, John Wiley & Sons, 1987.
19. D. C. Dunand, B. Q. Han, and A. M. Jansen, "Monkman-Grant Analysis of Creep Fracture in Dispersion Strengthened and Particulate-Reinforced Aluminum, "*Metallurgical and Materials Transactions A;* **30A** (1999) 829-838